Acta Materialia 105 (2016) 417–428

Contents lists available at ScienceDirect

Acta Materialia

journal homepage: www.elsevier.com/locate/actamat

Full length article

A study of deformation twinning in a titanium alloy by X-ray diffraction contrast tomography

Laura Nervo [a, b], Andrew King [d], Arnas Fitzner [a], Wolfgang Ludwig [b, c], Michael Preuss [a, *]

[a] Materials Science Centre, The School of Materials, University of Manchester, Oxford Road, Manchester M13 9PL, United Kingdom
[b] ESRF – The European Synchrotron, 71 Rue des Martyrs – CS 40220, 38043 Grenoble, France
[c] MATEIS, INSA de Lyon, Université de Lyon, 7 Avenue Jean Capelle, 69621 Villeurbanne, France
[d] Synchrotron SOLEIL, L'Orme des Merisiers Saint-Aubin – BP 48, 91192 GIF-sur-YVETTE, France

ARTICLE INFO

Article history:
Received 5 November 2015
Received in revised form
12 December 2015
Accepted 15 December 2015
Available online 9 January 2016

Keywords:
Deformation twinning
Slip transfer
Titanium alloys
X-ray diffraction contrast tomography
Neutron diffraction

ABSTRACT

A specimen of Ti–4Al deformed in-situ to about 0.7% compressive strain using neutron diffraction, and showing early stages of twinning, has been investigated in 3D using synchrotron X-ray diffraction contrast tomography (DCT). A cylindrical volume of 900 μm × 400 μm diameter was observed using DCT, containing about 400 grains of which almost 60 grains were identified to have twinned predominantly by $\{10\bar{1}2\}\langle\bar{1}011\rangle$ 011 tensile twinning. To consider possible twin nucleation criteria, non-twinned grains of similar orientation to the twinned grains were compared against the family of twinned grains. Such comparison highlights that the twinned grain family has a grain size distribution shifted to a higher mean value than the corresponding family of grains that has not twinned. An initial neighbourhood analysis did not reveal any significant differences of the two grain families. However, complex twin chains and clusters were identified forming a slightly imperfect network demonstrating the importance of the 3D analysis. Analysis of the parent grain orientations within those chains/clusters using the Luster-Morris parameter revealed a significantly higher propensity of prismatic $\langle a\rangle$ slip transfer compared to the neighbourhood of the non-twinned grain family while no difference was observed for the likelihood of twin shear transfer. The findings suggest that grain chains/clusters with high ability of prismatic $\langle a\rangle$ slip activity and slip transfer does promote formation and clustering of twins, which is likely associated with the build up of tensile intergranular strain along the $\langle c\rangle$ axis perpendicular to the loading direction recently suggested by crystal plasticity modelling.

1. Introduction

Metals with a hexagonal close-packed (HCP) crystal structure, such as Ti, Mg and Zr, are known to display easy $\langle a\rangle$ slip, either on the prismatic or basal plane. In the case of titanium, the most common slip mode is $\{10\bar{1}0\}\langle 1\bar{2}10\rangle$ prismatic slip while pyramidal $\langle c+a\rangle$ slip has been observed but only in small fractions [1–3]. This is due to pyramidal $\langle c+a\rangle$ slip having a critical resolved shear stress (CRSS) at room temperature about 3–5 times higher than for prismatic $\langle a\rangle$ slip [4,5]. However, plasticity that provides shear with a $\langle c\rangle$ component is necessary to achieve significant plastic deformation in polycrystalline titanium [6]. This is because the $\{10\bar{1}0\}\langle 1\bar{2}10\rangle$ prismatic slip mode alone is not sufficient to accommodate an arbitrary plastic strain, which requires five independent slip systems [7], according to the von Mises criterion [8].

More recent work has demonstrated that plasticity in polycrystalline materials can be accommodated by fewer independent slip systems per grain [1] but, in the absence of easy slip including a $\langle c\rangle$ component, twinning is commonly observed in Ti and other metals with an HCP crystal structure. This is particularly the case during compression loading [9–16]. For example, twinning can provide the majority of plastic deformation in Mg alloys, if the starting texture promotes grains ideally orientated for twinning but not for $\{0001\}\langle 1\bar{2}10\rangle$ basal slip [17–24].

In hexagonal titanium, four different twinning modes have been reported [11]. At room temperature, the predominant twinning mode is the $\{10\bar{1}2\}\langle\bar{1}011\rangle$ tensile twin [25–28,6,29,30,22,31], which corresponds to a rotation of 85° around the $\langle 11\bar{2}0\rangle$ axis. In

* Corresponding author.
E-mail addresses: laura.nervo@esrf.fr, laura.nervo84@gmail.com (L. Nervo), king@synchrotron-soleil.fr (A. King), arnas.fitzner@brunel.ac.uk (A. Fitzner), ludwig@esrf.fr, ludwig@insa-lyon.fr (W. Ludwig), michael.preuss@manchester.ac.uk (M. Preuss).

http://dx.doi.org/10.1016/j.actamat.2015.12.032

some cases, this twin mode has been observed to result in almost complete grain reorientation after only modest levels of strain [32–38].

Statistical analysis of twin nucleation in hexagonal metals has suggested that twin activation does not necessary follow the traditional Schmid law, meaning that in some cases the twin variant that forms is not the one with the highest Schmid factor [35,23,39]. However, more recent work has demonstrated that once the local stress state is taken into account by the use of a crystal plasticity model, the twin variant selection follows the stress criterion [40]. The applied stress is expected to play an important role in twin nucleation, as discussed in Yoo [1] and Meyers et al. [12]. In general, they state that the applied stress is proportional to the number of twins per unit of observed area, as found similarly in Chichili [33]. This applied stress is an average resolved stress and is a rather crude approximation. To understand the increasing density of twins with increasing levels of applied stress there can be two scenarios: (i) the stress is considered as uniform field applied on an array of potential twin nucleation sites, in which the increasing levels of applied stress allow more sites to be activated; (ii) the critical stress for nucleation is met only at the most potent of the stress concentrations. When increasing the applied stress, more of the available stress concentrators provide stresses that attain the critical level. In most of the cases, the reality is most likely to correspond to a combination of these two scenarios.

Localised slip resulting in dislocation pile up at grain boundaries has also been found to play a role in twin nucleation, which has been recently investigated in commercially pure titanium grade 1 [41–44], together with the free surface relaxation and non-Schmid stress effects on twin nucleation [45]. The slip activity in a grain well aligned for prismatic $\langle a \rangle$ slip leading to twin nucleation in a neighbouring grain not well aligned for $\langle a \rangle$ type slip was shown to be significant when a tensile stress state was created [42]. Twin to twin shear transfer across grain boundaries has also been observed, particularly in boundaries with misorientations lower than 30° [41]. These correlations were quantified using the slip transfer parameter *m'*, which was first introduced by Luster and Morris [46] based on observations by Clark et al. [47].

Numerous deformation studies on metals with a HCP crystal structure have used in-situ loading in combination with neutron diffraction to study intergranular strain evolution of various grain families [48–53]. When carrying out compression loading such approach also enables easy detection of $\{10\bar{1}2\}\langle\bar{1}011\rangle$ twinning as the $\langle c \rangle$ axis tends to rotate into the loading direction, which is monitored by measuring the {0002} integrated peak intensity. This method is particularly useful to compare twin activities and enables one to capture the moment of early twin formation.

Considering the importance of neighbourhood in relation of twinning, several synchrotron X-ray techniques might be of particular interest as they enable 3D analysis of polycrystalline materials non-destructively. Examples here are the differential aperture X-ray microscopy (DAXM) approach that was developed at the advanced photon source (APS) by a group from the Oak Ridge National Laboratory USA [54–57] and far-field 3D X-ray diffraction (3DXRD), which was first developed at Risø DTU in Denmark [58–62].

X-ray diffraction contrast tomography (DCT) [63,64] is a variant of the 3DXRD microscopy technique enabling simultaneous reconstruction of the 3D microstructure (shape and orientation) in suitable polycrystalline materials, along with the absorption map of the specimen. The X-ray DCT methodology provides access to the 3D shape, orientation and elastic strain state of the individual grains from polycrystalline materials fulfilling some conditions in terms of grain size and intergranular orientation spread.

In the present work the onset of twinning is studied in a binary Ti–4Al alloy, using two different diffraction techniques, neutron diffraction and X-ray DCT. Samples were first compressed and the activation of $\{10\bar{1}2\}\langle\bar{1}011\rangle$ tensile twins was followed in-situ by means of neutron diffraction.

Subsequently, small samples were extracted from the deformed samples (about 0.04% of the initial sample volume) at selected applied strains, and characterised using the X-ray DCT methodology to reveal the 3D grain structure, allowing a grain-by-grain study of the shape and location of twins. A statistical analysis was carried out in which the parent grains of twins where grouped together and compared with similarly orientated grains that had not twinned. Comparisons were carried out regarding grain size, the general Schmid factor *m* (based on an uniaxial stress) [65] and slip transfer parameter *m'* [42,66–68] across the grain boundaries. Finally, a search for possible clustering of twins was carried out and cluster neighbourhoods were again analysed.

2. Experimental procedure

2.1. Material preparation

For the purpose of this research, 200 g binary Ti–4Al (i.e. 4wt.%) alloy buttons were double melted in a tungsten arc furnace under inert gas atmosphere. Each button was beta forged at 1100 °C at the TIMET research facility in Witton, UK. The measured chemical composition of the alloy is given in Table 1. Subsequently, the buttons were cross-rolled in bar shape (14 × 14 × 260 mm) on a "2 high Robertson mill" (WHA Robertson & Co Ltd) at 870 °C followed by a recrystallization (RX) heat treatment at 993 °C (30 °C below the beta transus temperature) in a tube furnace under Argon shielding for 5 h followed by air-cooling. The lattice parameters and the c/a ratio were determined at the neutron spallation source ISIS, Chilton, UK. They are $\langle a \rangle = 2.935$ Å and $\langle c \rangle = 4.678$ Å giving a c/a ratio of around 1.5938 [69]. The average grain size of the studied samples is 73 μm, which was measured by using the linear intercept method [69]. The {0002} pole figure and the initial microstructure of the Ti–4Al raw material used in this analysis is shown in Fig. 1.

Three samples with a diameter of 5 mm and length of 12.35 mm each were cut by electro-discharge machining (EDM) with the cylinder axis parallel to the original rolling direction (RD). The texture of the material is such that the $\langle c \rangle$ axes of the grains tend to be oriented perpendicular to the cylinder axis, which promotes tensile twinning during compression loading as the $\langle c \rangle$ axis is strained in tension.

2.2. In-situ loading using neutron diffraction

In the first part of the experiment, each sample was placed in a stress-rig based on the Strain Analyser for Large and Small scale engineering Applications (SALSA) beam line at the Institut Laue-Langevin (ILL) in Grenoble, France [70,71]. It uses a thermal neutron beam with wavelength $\lambda = 1.62$ Å corresponding to a two-theta angle of 40.5° for the {0002} reflection for Ti–Al alloy, which was measured in the loading direction. The two-dimensional position sensitive micro-strip detector has an active area of 80 × 80 mm^2 with 256 × 256 channels and was positioned in a way that the scattering vector q of the {0002} reflection was parallel to the loading direction. The angle covered by each channel is 0.02° at a sample-detector distance of 1 m. The 2D data were integrated to produce a one-dimensional diffraction peak profile covering 5°, in which the {0002} and $\{10\bar{1}1\}$ peaks are visible, and fitted using a Gaussian function. Because of the poor neutron scattering properties of Ti the counting time per load step was 30 min in order to obtain a fittable {0002} reflection. As the main concern was the

Table 1
Chemical composition of Ti–4Al.

Al		C	N_2	O_2	Ti
3.9 wt.%	6.7 at.%	50 ppm	23 ppm	778 ppm	bal.

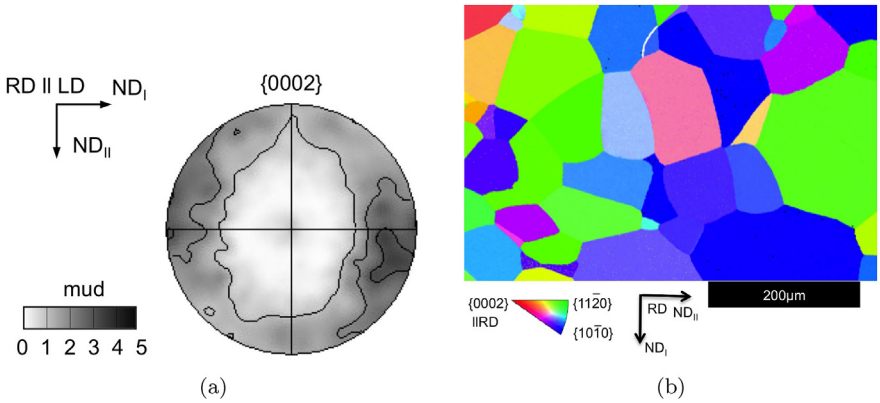

Fig. 1. Initial microstructure of the material represented in terms of (a) {0002} pole figure and (b) grain orientation map recorded by EBSD.

plastic strain induced at each load step, the sample was placed in displacement control while acquiring the neutron diffraction data to avoid cold creep. The load increments were carried out using a strain rate of 0.004 s^{-1}.

Initially, a sample was deformed reaching about 6.4% compressive strain and the evolution of the integrated intensity of the {0002} reflection was monitored. Based on the initial observation, two more samples were deformed up to the onset of deformation twinning and cut subsequently by EDM to extract small cylindrical samples of 400μm diameter and 3 mm length for the X-ray DCT measurement. These small samples share the same cylinder axis as the sample from which they were extracted.

2.3. Diffraction contrast tomography (DCT)

The second part of the experiment was performed at the beam line ID11 of the ESRF, The European Synchrotron (Grenoble, France), using a monochromatic beam produced by a bent Si (111) Laue–Laue double-crystal monochromator (40 keV, wavelength $\lambda = 0.309$ Å, relative bandwidth $\Delta\lambda/\lambda \approx 10^{-3}$). The experimental setup is represented schematically in Fig. 2. A high resolution detector system consisting of a Fast Readout Low Noise (FReLoN) charge-coupled device (CCD) camera [72] equipped with a scintillator screen and visible light microscope optic was used for this experiment, positioned normal to the incident beam, about 5 mm downstream from the sample. The detector has an array of 2048×2048 pixels with an effective pixel size of 1.4μm/pixel and an active area of 2.87×2.87 mm^2. An absorber was inserted between the sample and the detector to attenuate the transmitted beam without affecting the diffracted beams. This allows the integration time per image to be increased to improve the intensity particularly of weak diffraction spots (i.e. the ones related to this twin lamellae).

2.4. Data analysis

The standard X-ray DCT analysis methodology has previously been described in detail [63,64]. A series of images (typically 3600–7200) are recorded while the sample is rotated through 360°. The background is subtracted from the images, leaving only the diffraction spot images. These are segmented, and metadata are recorded that describe the spots. The geometry of diffraction events is extracted using a Friedel pair geometry, based on identifying pairs of spots arising from the scattering vector and same grain, offset by 180° rotation of the sample. The Friedel pair construction reveals the diffraction angles and scattering vector associated with the diffraction event, and a path through the sample on which the grain must lie. Grain positions and orientations are identified by searching for Friedel pairs that are spatially and crystallographically consistent. The grain shapes are then reconstructed using a simultaneous iterative reconstruction technique (SIRT) algorithm, using the diffraction spot images as grain projections. Subsequently, the grain shapes are assembled to produce a 3D grain map. Any overlapping or unassigned spaces in the 3D map are filled using a morphological dilation.

Twinned microstructures present a significant challenge for the DCT methodology. The plastic deformation associated with the applied strain tends to introduce mosaicity in the crystal lattice of the grains, blurring and distorting the diffraction spot shapes. In addition, the mechanical twins formed during compression have a characteristic thin plate-like shape and a small volume, particularly at the onset of twinning, which poses difficulties for several reasons. The low volume means that the spot intensities are generally low, and difficult to segment from the background. The high aspect ratio means that different diffraction spots arising from a twin may have very different shapes, depending on the diffracted beam direction (projection direction).

As a result, the number of reflections assigned to parents and twins can vary a lot, with the one for twins being typically significantly smaller than the one for parents. For the experimental conditions used in this study typical numbers of assigned reflections were around 10–15 for twins, compared to 60–70 for the parent grains. The integrated diffraction spots were assembled into a stack of projections (sinogram) and stored together with the parameters defining the projection geometry.

An iterative tomographic reconstruction process was performed using an implementation of the SIRT algorithm available in the All Scale Tomographic Reconstruction Antwerp (ASTRA) tomographic toolbox [73,74]. The process assumes that all grains can be indexed in the volume and remaining gaps in this initial grain map are

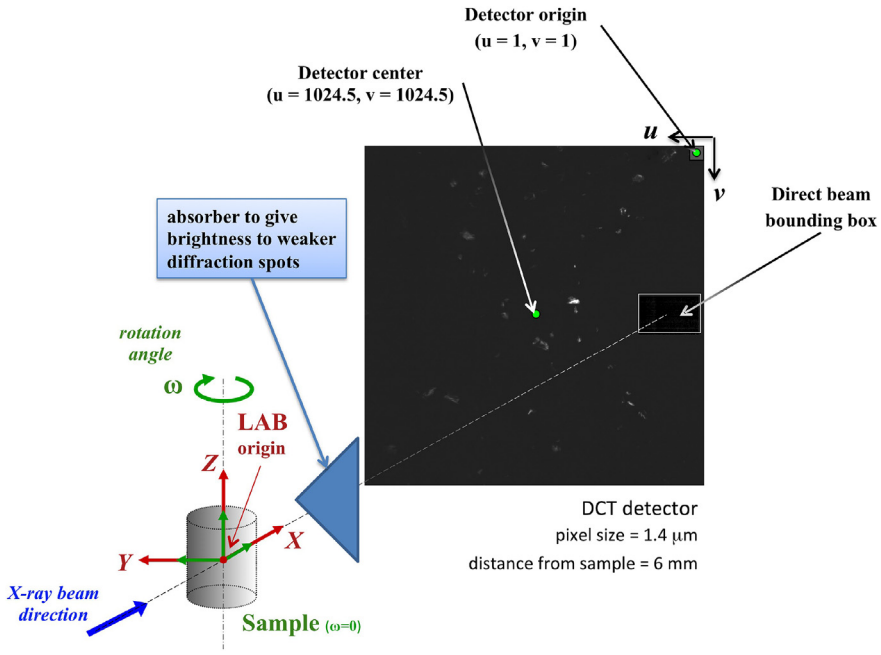

Fig. 2. X-ray DCT experimental setup used at the beam line ID11 of the ESRF, Grenoble, France. The coordinate system is defined such that the X-ray beam is along the laboratory X direction, the Z direction is vertical, upwards from the origin and the Y direction is consistent with a right-handed system. The rotation axis of the sample is right-handed and parallel with the z-axis. The sample coordinate system rotates around the z-axis and it coincides with the laboratory coordinate system when the rotation angle ω is equal to zero.

removed by dilating the existing grains until a space filling grain map is obtained.

X-ray DCT data were acquired for a couple of samples compressed to about 0.7% and to 1.5% plastic strain respectively. An absolute measure of the illuminated sample volume (V_{sample} = 0.0757mm^3) was obtained from the tomographic reconstruction of the transmission images recorded during the scan. The sample strained to 1.5% displayed significant reconstruction artefacts owing to limitations of the 3D analysis code, based on a single (grain average) orientation in the iterative algebraic reconstruction process and has been omitted here. However, the volume of the sample deformed to 0.7% plastic strain was reconstructed successfully using the DCT code. To identify the expected $\{10\bar{1}2\}\langle\bar{1}011\rangle$ tensile twins an automated search was carried out to identify grains overlapping in space and fulfilling the orientation requirements of any of the twinning modes for hexagonal titanium and then the $\{10\bar{1}2\}\langle\bar{1}011\rangle$ tensile twinning mode was selected (the angle between the $\langle c\rangle$ axis of two grains must be 85° and the rotation axis parallel to one of the six $\langle 11\bar{2}0\rangle$ directions). The available slip systems and twin systems for HCP materials are listed in Table 2.

One particular point of interest in the analysis of the volume was the Luster-Morris parameter, which can be used to describe relative alignment of neighbouring grains in respect of certain planes and directions. It is defined by eq. (1) and illustrated schematically in Fig. 3.

$$m\prime = \cos\kappa \cos\psi \quad (1)$$

where ψ is the angle between two plane normals and κ is the angle between the associated slip/shear directions. Hence, m'=1 indicates perfect alignment of two neighbouring grains for easy slip transfer across the grain boundary. In the present work the Luster-Morris parameter was considered for neighbouring grains aligned for prismatic to prismatic slip transfer and $\{10\bar{1}2\}\langle\bar{1}011\rangle$ twinning shear to $\{10\bar{1}2\}\langle\bar{1}011\rangle$ twinning shear transfer between neighbouring grains.

Table 2
Deformation slip and twinning modes in hexagonal titanium [1,11,75,2,31,42]. For the deformation twinning modes we are using the $K-\eta$ notation adopted by Bilby and Crocker [26], p. 242]. ε is the shear strain.

Slip mode	Plane	Direction	Multiplicity
Basal $\langle a\rangle$	{0001}	$\langle 11\bar{2}0\rangle$	3
Prismatic $\langle a\rangle$	$\{10\bar{1}0\}$	$\langle 11\bar{2}0\rangle$	3
Pyramidal $\langle a\rangle$	$\{10\bar{1}1\}$	$\langle 11\bar{2}0\rangle$	6
Pyramidal $\langle c+a\rangle$ 1st ord	$\{10\bar{1}1\}$	$\langle 11\bar{2}3\rangle$	12
Pyramidal $\langle c+a\rangle$ 2nd ord	$\{11\bar{2}2\}$	$\langle 11\bar{2}3\rangle$	6

Twinning mode	K_1	η_1	Angle − axis	ε
Tensile Type I	$\{10\bar{1}2\}$	$\langle\bar{1}011\rangle$	85°$\langle 11\bar{2}0\rangle$	0.171
Tensile Type II	$\{11\bar{2}1\}$	$\langle\bar{1}\bar{1}26\rangle$	35°$\langle 1\bar{1}00\rangle$	0.629
Compression Type I	$\{11\bar{2}2\}$	$\langle 11\bar{2}3\rangle$	65°$\langle\bar{1}100\rangle$	0.221
Compression Type II	$\{10\bar{1}1\}$	$\langle\bar{1}012\rangle$	54°$\langle\bar{1}2\bar{1}0\rangle$	0.101

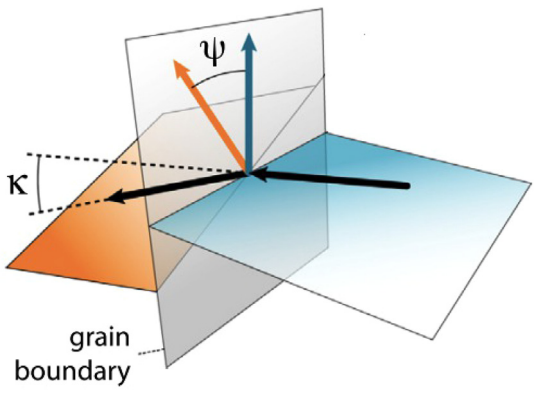

Fig. 3. Schematic description of the Luster-Morris parameter showing horizontal (orange and blue) planes (slip or twinning planes) on either side of the boundary. ψ is the angle between plane normals and κ is the angle between specific directions (slip or twin shear) [67]. (For interpretation of the references to colour in this figure legend, the reader is referred to the web version of this article.)

3. Results

Fig. 4 displays the change of integrated intensity of the {0002} peak relative to the initial value monitored in the loading direction as a function of plastic strain. It can be seen that the integrated intensity does increase from about 0.4% plastic strain (dashed line), which is indicative of $\{10\bar{1}2\}\ \langle\bar{1}011\rangle$ tensile twinning. Further, based on the evolution of the integrated intensity as a function of plastic strain, twinning activity appears constant over the tested range. Based on this observation, a second and third sample were compressed in-situ to 0.7% (blue line) and 1.5% plastic strain and neutron diffraction data confirmed early signs of twinning in both cases.

Both deformed samples were scanned using X-ray DCT but so far only the volume of the sample strained to 0.7% plastic strain has been reconstructed successfully. The reconstructed volume, together with the volume of the twinned grains only, is presented in Fig. 5a and b. In both figures grains are coloured according to the inverse pole figure scheme with the sample loaded along (0001), Fig. 5c.

The reconstructed grain volumes were dilated using a mask determined from absorption tomography to fill the empty spaces between the grains (a single grain dilation of maximum 7 μm has been used). The reconstructed sample volume, resulting from concatenation of 3 DCT scans, has resulted in a height of 0.77 mm and a volume of about 0.0757mm^3. The total number of grains in the studied volume is 402, out of which 58 have twinned (some of them containing multiple twins) and 67 of the 70 indexed twins have been identified as $\{10\bar{1}2\}\ \langle\bar{1}011\rangle$ tensile twins ($\approx$ 17% with respect to the total number of indexed grains).

The crystallographic orientations of the 402 grains are presented in form of an inverse pole figure map in Fig. 6, distinguishing between twinned grains, twins and grains that did not twin. It can be stated that the twinned grains (squares) are distributed uniformly in the region between $(10\bar{1}0)$ and $(2\bar{1}\bar{1}0)$ poles. Fig. 6 also highlights that the studied volume contains plenty of grains without twins that are similarly orientated to the grains that have twinned. In order to compare twinned and non-twinned grains in a meaningful way, each twinned grain was paired with the most similarly orientated grain that had not twinned, as shown in Fig. 6. This was achieved by calculating a distance in the orientation space between individual twinned grains and non-twinned grains. The orientation space is defined by two angles, the azimuthal angle ϕ and the polar angle ψ, which both describe the inverse pole figure. In order to consider a non-twinned grain of similar crystallographic orientation to a twinned grain, the distance d between a twinned grain with coordinates (ϕ_i, ψ_i) and a grain that had not twinned with coordinates (ϕ, ψ) had to satisfy:

$$d = \sqrt{(\phi_i - \phi)^2 + (\psi_i - \psi)^2} < 1.5^\circ \quad (2)$$

This tight criterion was chosen to ensure that single solutions could be found for each twinned grain. Following this procedure, 43 similarly oriented grains were found corresponding to twinned grains over a total of 58 twinned grains. Hence, 15% of the twinned grains could not be paired with a non-twinned grain.

The analysis of the twinned grains revealed that 96% of the characterised deformation twins in the sample were $\{10\bar{1}2\}\ \langle\bar{1}011\rangle$ tensile twins, i.e. 67 $\{10\bar{1}2\}\ \langle\bar{1}011\rangle$ tensile twins, one $\{11\bar{2}1\}\ \langle\bar{1}\bar{1}26\rangle$ tensile twin and two $\{11\bar{2}2\}\ \langle11\bar{2}3\rangle$ compression twins. The distribution of the misorientation angle between the twinned grains and the $\{10\bar{1}2\}\ \langle\bar{1}011\rangle$ tensile twins is shown in Fig. 7 showing an average misorientation angle of 85.3°, which is 0.3° above the theoretical value for this type of twin in pure Ti, Table 2.

In a first step of comparing the twinned grain family with the one that had not twinned but was of comparable crystallographic orientation, Fig. 8 compares the number of grain neighbours for the two different families in form of a cumulative plot.

This analysis immediately highlights that the twinned grains have in average a significantly higher number of grain neighbours than the related grain family that has not twinned yet. Following on from this observation, the grain volume for each grain has been computed directly from the reconstructed sample, before and after dilation, as shown in Fig. 9a and b, respectively. It should be noted that the volume of a twinned grain combines the parent grain and the twin volume.

It can be noted that the difference of grain volume before and after dilation is not significant. Most importantly, the volume dilation does not appear to create artefacts justifying the use of the dilated volume for each grain as a measurement of the grain volume. Consequently, Fig. 9 clearly demonstrates that the grain volume distribution of the twinned grain family is shifted to a larger volume than the grains without twins. Hence, the grain volume analysis suggests that during the very early stage of plasticity grain size is an important factor for twin nucleation and growth.

During the next stage, the grain neighbourhood of the two grain families was investigated in greater detail. First of all it is important to note that during compression loading and considering the starting texture, the grains that are most likely to twin are also well aligned for deformation by prismatic $\langle a\rangle$ slip. Hence, a neighbourhood that displays a high Schmid factor of similar orientation is more likely to allow the twinning grain to build up a high dislocation density and large intergranular strains, i.e. large tensile strains along the $\langle c\rangle$ axis perpendicular to the compressive loading axis. Both these aspects could be considered to promote $\{10\bar{1}2\}\ \langle\bar{1}011\rangle$ twin nucleation. Fig. 10 plots the prismatic $\langle a\rangle$ slip Schmid factor distribution computed for the grain neighbourhood of both grain families. It can be seen that both grain families display a high fraction of grain neighbours well aligned for prismatic $\langle a\rangle$ slip but there is no noticeable difference in Schmid factor distribution between the two.

In addition, Fig. 10 exhibits the distribution of the transfer parameter m' for prismatic $\langle a\rangle$ slip computed from the neighbourhood of the two different grain families. It is noticeable that both grain families display a wide distribution of m' but the analysis again does not yield a clear differentiation between the twinned grains and the grains that have not twinned yet after 0.7% plastic

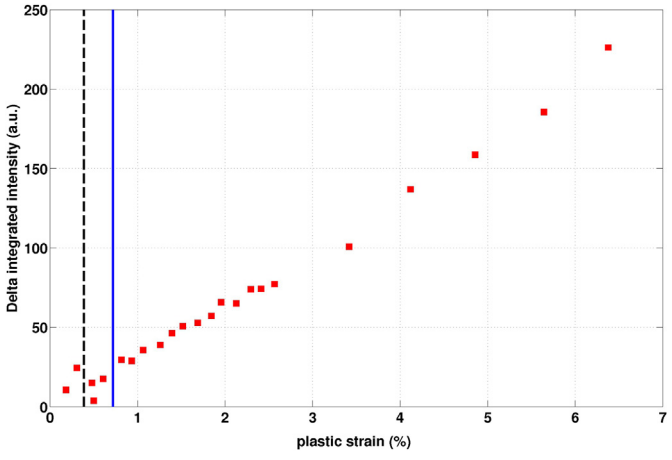

Fig. 4. Change of {0002} integrated intensity as a function of plastic strain recorded during in-situ loading on SALSA, at the ILL, Grenoble. Early signs of twinning by slight increase of intensity can be seen just below 1%.

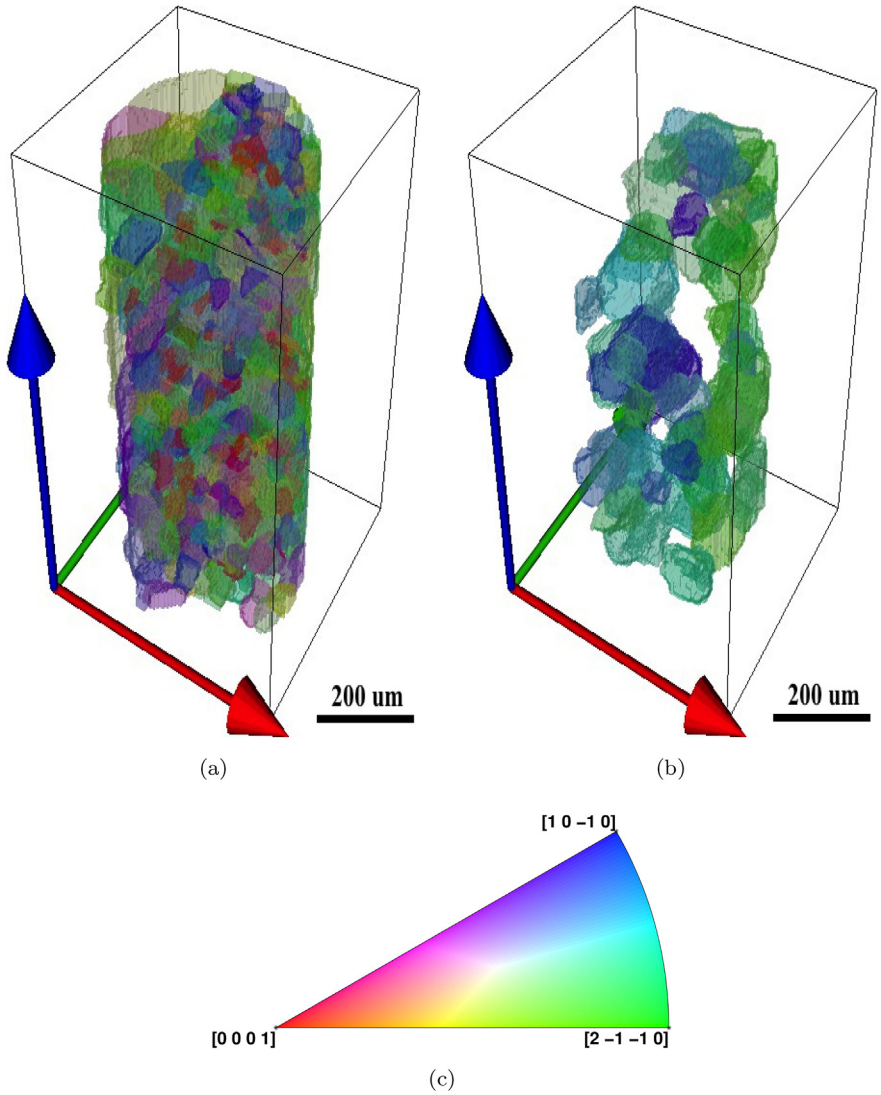

Fig. 5. 3D grain map of the reconstructed sample volume coloured according to the inverse pole figure (IPF) colour code for HCP materials (c). Full 3D grain maps of (a) all the grains and (b) only twinned grains are displayed. (For interpretation of the references to colour in this figure legend, the reader is referred to the web version of this article.)

deformation.

It is also potentially important to consider the ability of the grain neighbourhood to accommodate the shear strain generated by a twin. This might be best accommodated by twin nucleation in a neighbouring grain and hence Fig. 11 plots the Schmid factor distribution for $\{10\bar{1}2\}\langle\bar{1}011\rangle$ tensile twinning of the neighbourhood assuming a stress criterion for twinning while the transfer parameter *m'* for $\{10\bar{1}2\}\langle\bar{1}011\rangle$ tensile twins is plotted in Fig. 11. Again, both neighbourhoods display a high fraction of neighbouring grains well aligned for $\{10\bar{1}2\}\langle\bar{1}011\rangle$ tensile twinning but also an almost identical distribution. Further, both grain families show a relatively sharp distribution of very high *m'* values indicating that the grain neighbourhood is well aligned for shear transfer by $\{10\bar{1}2\}\langle\bar{1}011\rangle$ tensile twinning. However, no distinction can be drawn between the two different grain families.

As a next step, a more detailed analysis of the position of the twinned grains was carried out within the studied volume with the purpose of identifying potential chains or clusters of twinned grains and perform a neighbourhood analysis on these. Fig. 5 had already indicated that twinned grains are not isolated, but they form chains/clusters very close to each other. The individual twin chains/clusters are rendered in Fig. 12 using a different colour for each chain.

For clarity, Fig. 12b–f also highlight each individual chain. As this search indicated predominantly clusters rather than chains, the exact identification presented some difficulties. In this case a given twinned grain can have more than two neighbouring twinned grains, which makes the rendering of the neighbourhood more difficult. Each cluster was defined by starting from a grain with only one neighbouring twinned grain and the rendering did proceed by choosing the grain with the lowest number of neighbours among the neighbouring twinned grains, in order to simplify the choice as much as possible. As such search needs to be carried out in 3D space the calculation and the identification of the clusters was very computing intensive.

Among 58 twinned grains, 5 different clusters/chains were identified with the shortest cluster consisting of 6 twinned grains and the largest cluster containing 16 grains. In general, the twins linked up well within a cluster as demonstrated in Fig. 12b–f. In addition, only one isolated twinned grain was identified. It is also worth noting that a careful analysis of all the clusters/chains revealed that they seem to have formed a slightly imperfect

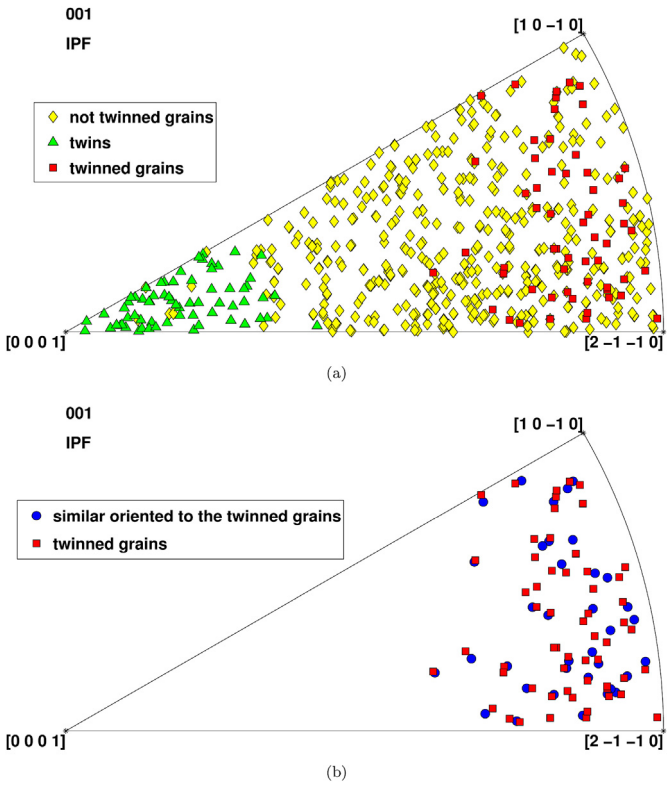

Fig. 6. Inverse Pole Figure (IPF) representation of the grain orientations with respect to the sample loading direction (001). In (a), all grains and twins are shown while in (b) only the two grain families, i.e. the twinned grains and their corresponding non-twinned similar oriented grains are shown.

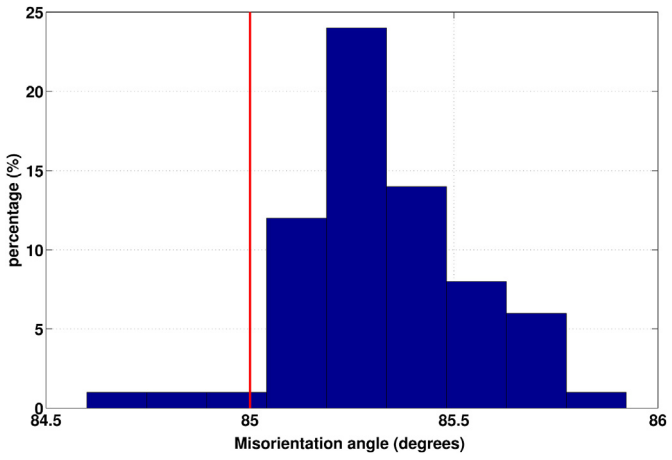

Fig. 7. Misorientation angle between the twinned parent grains and their tensile twins. The red line indicates the theoretical value of the misorientation angle (85°) for $\{10\bar{1}2\}\langle\bar{1}011\rangle$ tensile twin. (For interpretation of the references to colour in this figure legend, the reader is referred to the web version of this article.)

network, i.e. only small gaps are present between the clusters/chains. Finally, the transfer parameters for prismatic $\langle a\rangle$ slip and $\{10\bar{1}2\}\langle\bar{1}011\rangle$ tensile twinning were computed along those chains/clusters. The distributions (cumulative sum) of these two transfer parameters for the 16 grains/twins belonging to the longest chain are plotted in Fig. 13. It can be seen that m' for $\{10\bar{1}2\}\langle\bar{1}011\rangle$ tensile twinning within the chain never drops below 0.6 while the transfer coefficient for prismatic $\langle a\rangle$ slip within the chain shows a few

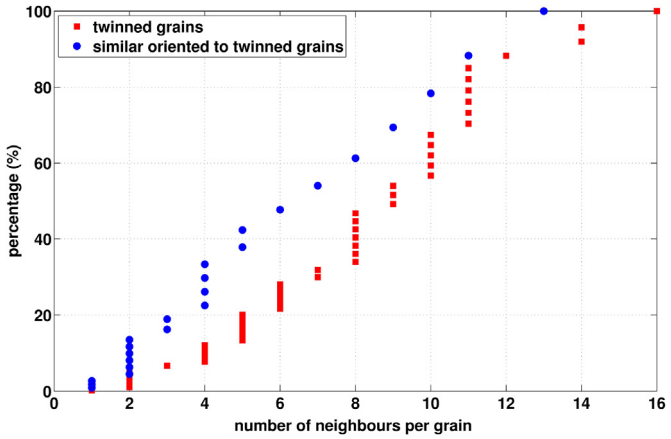

Fig. 8. Cumulative plot of the number of neighbours per grain for the twinned grains (squares) and the similarly oriented grains to the twinned grains (circles). The neighbours are computed from the reconstructed and dilated sample volume (shown in Fig. 5) and the surface grains have been removed from this calculation, in order to avoid any bias in the data.

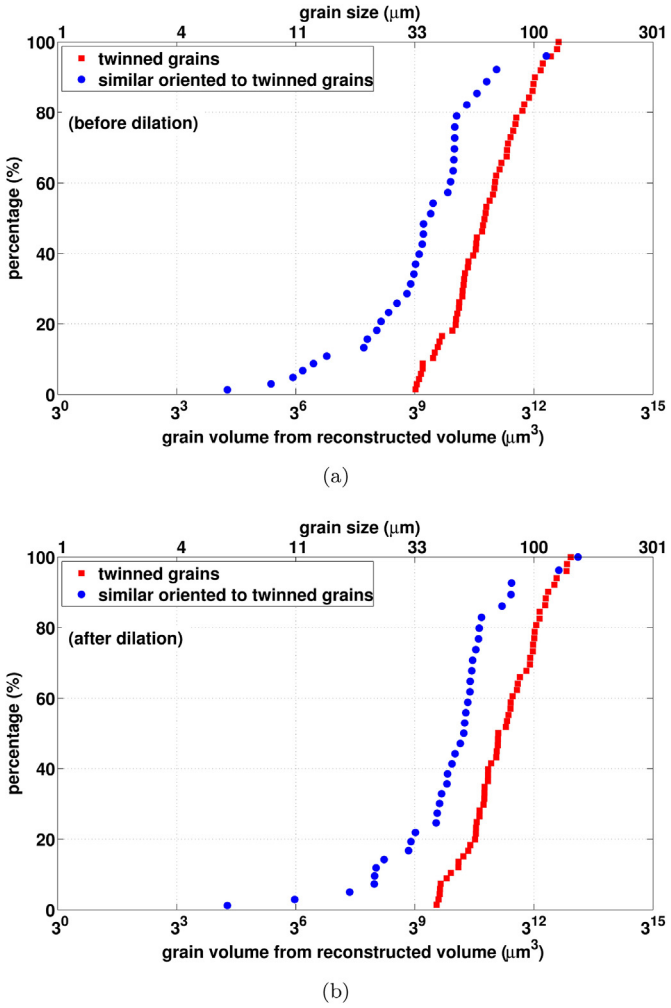

Fig. 9. Cumulative plot of the grain volume for the twinned grains (squares) and the similarly oriented grains to the twinned grains (circles), calculated from the reconstructed volume: (a) before dilation and (b) after dilation. The grain size is the diameter of the equivalent sphere corresponding to the grain volume and it is shown in the upper horizontal axis. A log scale in base 3 is used for both the horizontal axes.

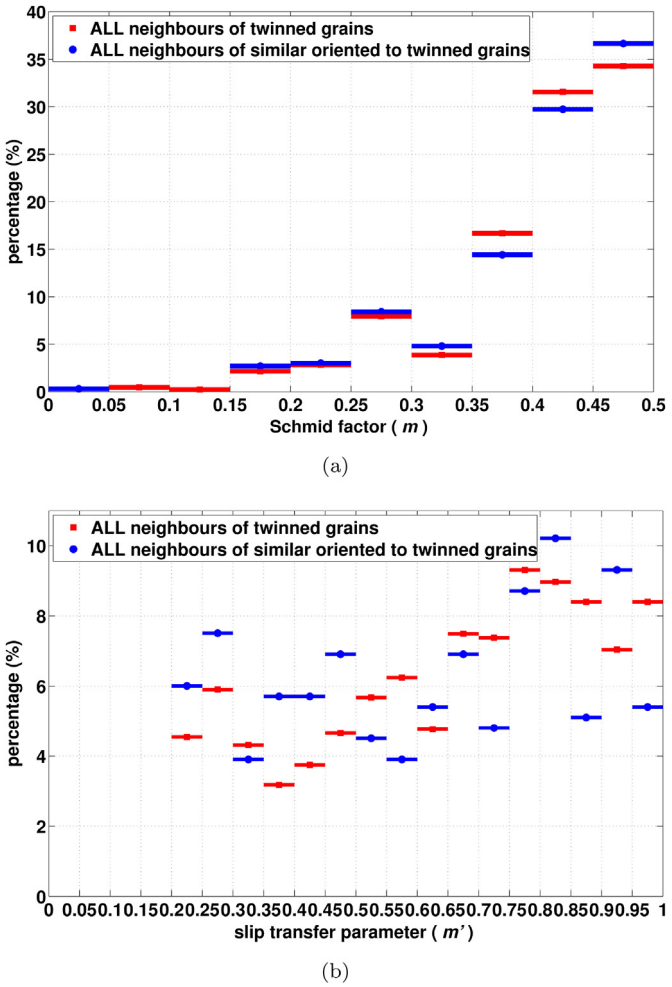

Fig. 10. (a) Schmid factor m for prismatic slip and (b) slip transfer parameter m' for prismatic slip to prismatic slip has been calculated for all the neighbours of the twinned grains (squares) and the similarly oriented grains to the twinned grains (circles).

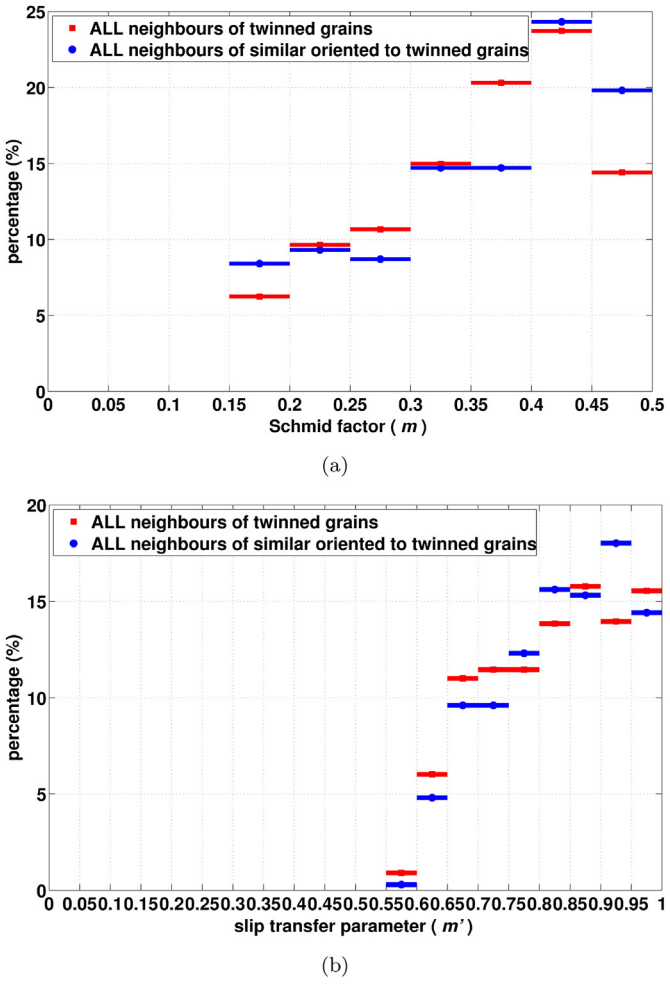

Fig. 11. Distribution of (a) Schmid factor m for $\{10\bar{1}2\}\langle\bar{1}011\rangle$ tensile twinning of the neighbourhood and (b) slip transfer parameter m' for $\{10\bar{1}2\}\langle\bar{1}011\rangle$ tensile twinning of the parent grain to $\{10\bar{1}2\}\langle\bar{1}011\rangle$ tensile twinning a neighbouring grain calculated for both grain families.

neighbours with a value around 0.25.

Fig. 14a and b displays the distributions of both transfer coefficients computed from within the chains/clusters and compare them with the previously computed transfer coefficient between the twin-free grain family and their neighbourhood. It should be noted that the main difference here to Figs. 10b and 11b for the twinned grains is that now only the transfer coefficients within clusters/chains are calculated whereas before simply all neighbours of a twinned grains were considered in the calculation. Such more local comparison reveals that within clusters/chains the grains are particularly well aligned for transferring prismatic $\langle a\rangle$ slip showing significantly higher m' values compared to the twin-free grain family, Fig. 14. In contrast, the m' of $\{10\bar{1}2\}\langle\bar{1}011\rangle$ tensile twinning within twin clusters/chains remains very similar to the twin-free grain family, Fig. 14.

4. Discussion

The results presented here clearly demonstrate that X-ray based diffraction contrast tomography is an excellent tool to undertake detailed analysis of twinned grains and their neighbourhood. It should be kept in mind that twins are detected by capturing the diffraction spot signals of the twin. Clearly, in the case of very thin twins, there is a high possibility that a twin is missed in the analysis. The thinnest twin detected in the present case was about 14μm wide for the thin twin face and occupied a volume of 1.2 $10^3\mu m^3$. Hence, one might assume that the present analysis captures the twins that formed first and have grown to a size that has made them detectable. An important aspect of the present work is that a sufficient number of twins were captured to undertake a statistical analysis of the neighbourhood and compare with similarly orientated grains that had not twinned. This analysis reveals a number of important drivers for early twin formation and that there is a tendency for the formation of twin clusters and chains, which seem to develop into a twin network, Fig. 12.

Regarding drivers for early twin formation, the 3D nature of the analysis has revealed the importance of grain size for early twin formation, Fig. 9. While positive grain size dependency of twinning has been reported previously for Mg [76], Ti [77] and Zr [35], the present 3D analysis provides a clear picture of size dependency within a single sample. It has been suggested previously that the reduction of twin activity in the case of small grains is related to the twin boundary energy cost being relatively high compared to the plastic work induced by the twin [78], p. 532]. It has also been suggested that the size effect is simply related to a decrease in the number of twins with decreasing grain size [79].

This consideration assumes the importance of grain boundaries

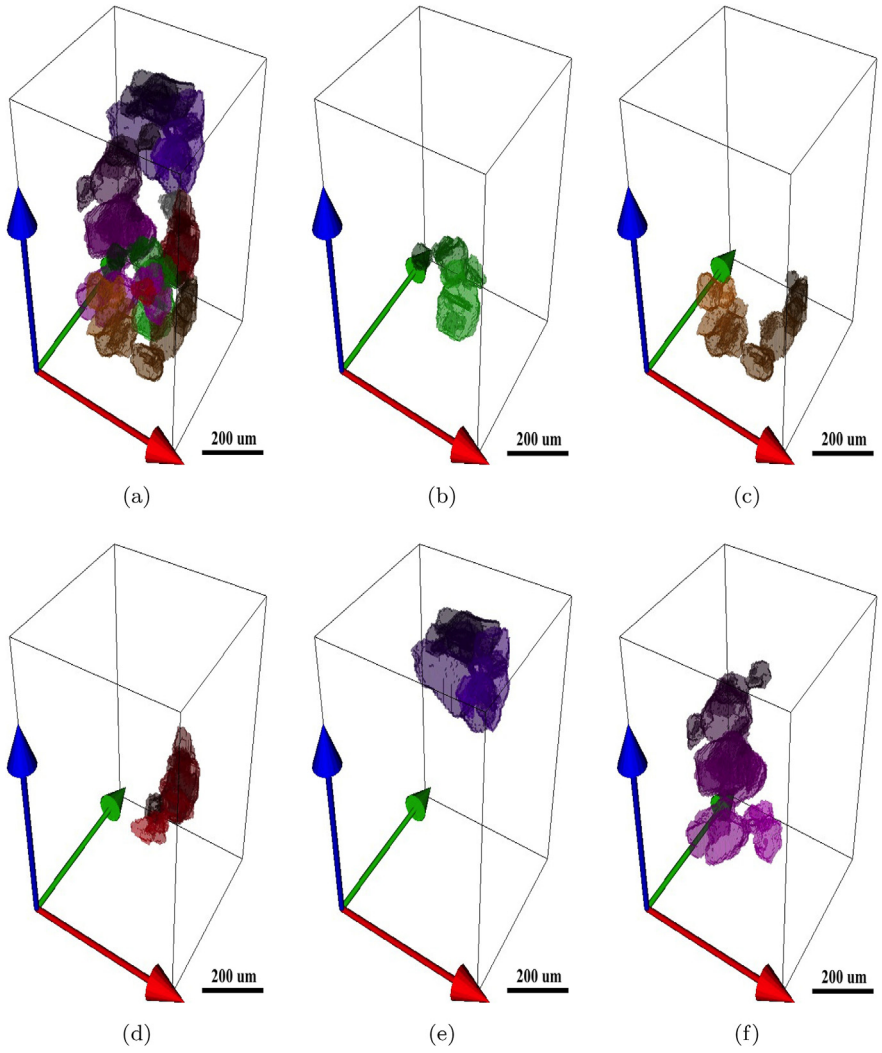

Fig. 12. (a) 3D rendering of the identified chains of twinned grains. (b) Each chain is visualised with a different colour and displayed in a separate figure. The darkest colour has been assigned to the first grain of the chain. (For interpretation of the references to colour in this figure legend, the reader is referred to the web version of this article.)

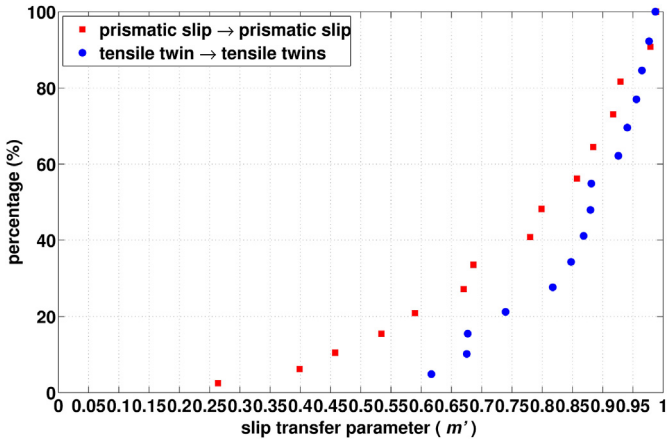

Fig. 13. Slip transfer parameter m' along the longest chain for prismatic slip to prismatic slip (squares) and for tensile twin to tensile twin (circles).

on twin nucleation. The true twin thickness has been found to be independent of grain size in magnesium and zirconium by Tomé and colleagues [23,35] but strongly dependent on the grain size in titanium [80]. In addition, they found that the number of twins in twinned grains increased with increasing grain size. Armstrong and Worthington [81] suggest that twinning is associated with microplasticity and high stress concentrations within local regions. As X-ray DCT might not capture the very early stage of twin formation, the observed grain size dependency could indicate easier growth of twins in comparatively large grains. The present observation of grain size dependency within a sample is interesting as it is reasonable to assume that large grains orientated well for prismatic $\langle a \rangle$ slip deform earlier than similarly orientated grains that are smaller, following the Hall-Petch relationship. Hence, significant intragranular strains would first develop in large grains (tensile intragranular strain along the transverse direction, i.e. parallel to the c-axis) and it might be those intragranular strains that promote twin formation.

An important factor regarding twin nucleation is also the stress acting on the grains during mechanical loading. It has been demonstrated previously that compression loading of Ti and Zr, with similar starting textures as in the present case, first result in deformation by slip before twinning is observed [82,27]. In this configuration, it is the 'soft' grains, i.e. grains well aligned for prismatic $\langle a \rangle$ slip, which are prone to form $\{10\bar{1}2\}\langle\bar{1}011\rangle$ tensile twins in order to relieve the tensile stress along the $\langle c \rangle$ axis

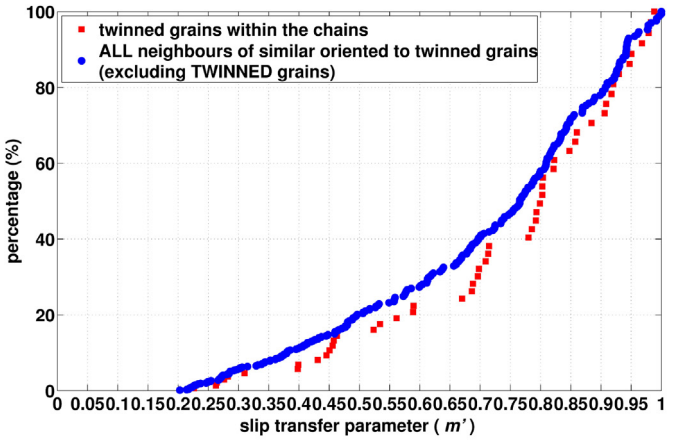

(a)

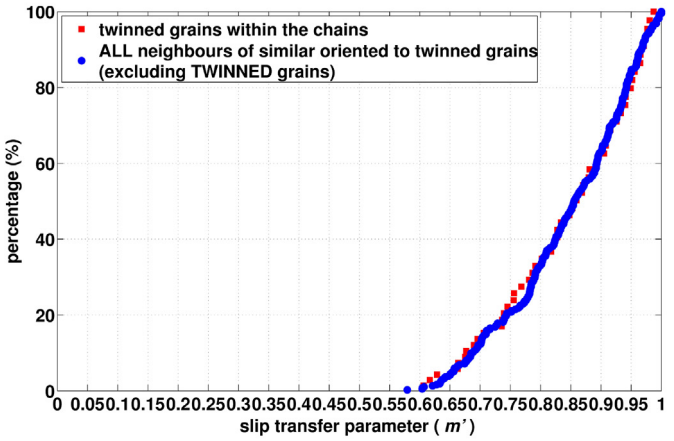

(b)

Fig. 14. Distributions of transfer parameter *m*' for (a) prismatic slip to prismatic slip and for (b) $\{10\bar{1}2\}\langle\bar{1}011\rangle$ tensile twin to $\{10\bar{1}2\}\langle\bar{1}011\rangle$ tensile twin for all the twinned grains of the chains (squares) and all the neighbours of the similarly oriented grains to the twinned grains (circles). The twinned grains are excluded from the neighbours of the similarly oriented grains.

generated in the transverse direction. It is also the configuration that tends to result in the highest twin activity when the material is deformed. Hence, one might argue that prismatic $\langle a\rangle$ slip activity is a critical parameter in order to induce sufficiently large intergranular strain along the c-axis to nucleate $\{10\bar{1}2\}\langle\bar{1}011\rangle$ tensile twins.

It should be noted that in a polycrystalline aggregate, the level of plasticity experienced by a grain does not necessarily depend on the global but the local stress state. For instance, a grain well orientated for prismatic $\langle a\rangle$ slip in respect of the applied loading direction but surrounded by grains well aligned for pyramidal $\langle c+a\rangle$ slip (hard orientation) will be shielded and is unlikely to experience high levels of plasticity. In contrast, if neighbouring grains are well aligned for prismatic slip and prismatic $\langle a\rangle$ 'slip transfer' across grain boundaries is possible, high levels of plasticity are likely in those grains. This will produce high intergranular strains, which could be a driver for twin nucleation. For this reason, the prismatic $\langle a\rangle$ slip transfer analysis is of importance here. While a simple comparison of the neighbourhood of all twinned grains with the neighbourhood of a similarly orientated non-twinned grain family did not show any differences, Fig. 10, considering only twin clusters/chains clearly demonstrated a *m*'-value distribution shifted to higher values, Fig. 14. Hence, the evolution of twin chains or clusters seems to be guided by following a chain/cluster of grains that can be linked by high prismatic $\langle a\rangle$ slip *m*'-values, i.e. a cluster of parent grains being well aligned for deforming first by prismatic $\langle a\rangle$ slip.

In contrast, a similarly sophisticated analysis of the transfer coefficient for $\{10\bar{1}2\}\langle\bar{1}011\rangle$ tensile twinning did not display a difference of values computed from within twin chains/clusters compared to calculating the transfer coefficient distribution of the related twin-free grain family and their neighbourhood, Fig. 14. This is interesting as one might argue that a shift towards higher *m*'-values within twin clusters/chains would have emphasised the importance of twins nucleating twins in neighbouring grains by creating stress concentrations [41,83,84,65,85]. As this concept should be most effective when the shear strain of the twinned grain is of similar direction as the twin shear strain induced in the neighbouring grain, i.e. high *m*'-value, the observations in Fig. 14 suggest that this mechanism only plays a minor role in the formation of twins in a polycrystalline aggregate with the given crystallographic texture.

Finally, it is worth emphasising that the present observations are relevant for compression loading and that the situation during tensile loading will be a very different one as in such case the $\{10\bar{1}2\}\langle\bar{1}011\rangle$ tensile twins form in grains that are not well aligned for any easy $\langle a\rangle$ slip [66].

5. Conclusions

A detailed analysis of a Ti–4Al sample compressed along the former rolling direction by only 0.7% plastic strain has been carried out first by using in-situ loading and neutron diffraction on SALSA, ILL, followed by X-ray Diffraction Contrast Tomography (DCT) on ID11, ESRF. The main purpose of this work was to study the onset of deformation twinning and consider the true grain neighbourhood in this 3D analysis in order to elucidate possible twin nucleation criteria. An important aspect of the analysis was to compare the family of twinned grains with a family of similarly orientated grains that had not twinned yet and identify key differences. The main findings can be summarised as follows:

- The neutron diffraction analysis enabled the early detection of $\{10\bar{1}2\}\langle\bar{1}011\rangle$ tensile twinning, which was seen after less than 1% plastic strain. A subsequent X-ray DCT analysis confirmed the dominance of $\{10\bar{1}2\}\langle\bar{1}011\rangle$ twins.
- The X-ray DCT analysis enabled the identification of almost 60 twinned grains with a few cases of multiple twins per grain within a sample volume of about 400 grains. It is important to note that it is possible that only twins that formed very early and have grown to an appreciable size were captured.
- A grain volume/size distribution analysis comparing twinned grains including the twin volume and similarly orientated grains that had not twinned revealed a clear shift towards a higher mean value in the case of the twinned grain family highlighting the importance of grain size on twin formation.
- An initial statistical analysis of the neighbourhood comparing the family of twinned grains with the crystallographically related non-twinned grain family did not reveal any significant differences.
- The 3D analysis revealed chains and clusters of twins that have also developed a slightly imperfect twin network. This suggests a strong neighbourhood effect.
- A Luster-Morris parameter analysis in respect of prismatic $\langle a\rangle$ slip and twin shear within chains/clusters and in comparison to the neighbourhood of the non-twinned grain family revealed that the twin clustering is most likely related to easy prismatic $\langle a\rangle$ slip transfer between the parent grains that form the chains/clusters of twins. In principle, this finding is in good agreement

with Timár and Quinta da Fonseca [86], which predicts the formation of twin clusters and the role of ⟨*a*⟩ slip strain location in Mg. In contrast, easy shear transfer from $\{10\bar{1}2\}\langle\bar{1}011\rangle$ twins was not identified as important factor within the chains/clusters suggesting that twin nucleation by stress concentration from a neighbouring grain that has twinned is not a main driving force for twin formation.

Finally, it should be noted that the present observations are relevant for a compression experiment and that tensile loading is likely to give different results since in this case the twinning grain has a 'hard' orientation while during compression loading the twinning grain is in a 'soft' orientation in respect of slip.

Acknowledgements

The authors would like to thank Henry Proudhon (Mines Paristech, Paris, France), for his help with the 3D volume rendering using python scripts.

The authors are grateful to the SALSA beam line scientists for their experimental support as well as the ESRF for their beam time support. The project was supported financially by the Engineering and Physical Science Research Council (EPSRC) in the UK (EP/F020910/1) and the ESRF in Grenoble, France.

References

[1] M.H. Yoo, Slip, twinning, and fracture in hexagonal close-packed metals, Metall. Trans. A 12 (1981) 409–418.
[2] S. Zaefferer, A study of active deformation systems in titanium alloys: dependence on alloy composition and correlation with deformation texture, Mater. Sci. Eng. A 344 (2003) 20–30.
[3] F. Bridier, P. Villechaise, J. Mendez, Analysis of the different slip systems activated by tension in a α/β titanium alloy in relation with local crystallographic orientation, Acta Mater. 53 (2005) 555–567.
[4] C. Leyens, M. Peters (Eds.), Titanium and Titanium Alloys, Fundamentals and Applications, WILEY-VCH Verlag GmbH and Co. KGaA, Weinheim, Germany, 2003, http://dx.doi.org/10.1002/3527602119.
[5] J. Gong, A.J. Wilkinson, A microcantilever investigation of size effect, solid-solution strengthening and second-phase strengthening fora prism slip in alpha-Ti, Acta Mater. 59 (2011) 5970–5981.
[6] M.H. Yoo, J.R. Morris, K.M. Ho, S.R. Agnew, Nonbasal Deformation Modes of HCP Metals and Alloys : Role of Dislocation Source and Mobility, Metall. Mater. Trans. A 33 (2002) 813–822.
[7] U.F. Kocks, The relation between polycrystal deformation and single-crystal deformation, Metall. Mater. Trans. 1 (1970) 1121–1143.
[8] R. von Mises, Mechanik der plastischen Formänderung von Kristallen, Z. für Angew. Math. Mech. 8 (1928) 161–185.
[9] D. Hull, Effect of grain size and temperature on slip, twinning and fracture in 3% silicon iron, Acta Metall. 9 (1961) 191–204.
[10] R. Armstrong, I. Codd, R.M. Douthwaite, N.J. Petch, The plastic deformation of polycrystalline aggregates, Philos. Mag. 7 (1962) 45–58.
[11] J.W. Christian, S. Mahajan, Deformation Twinning, Prog. Mater. Sci. 39 (1995) 1–157.
[12] M.A. Meyers, O. Vöhringer, V.A. Lubarda, The onset of twinning in metals: a constitutive description, Acta Mater. 49 (2001) 4025–4039.
[13] A. Staroselsky, L. Anand, A constitutive model for hcp materials deforming by slip and twinning, Int. J. Plast. 19 (2003) 1843–1864.
[14] L. Capolungo, I.J. Beyerlein, Nucleation and stability of twins in hcp metals, Phys. Rev. B 78 (2008) 024117.
[15] R.J. McCabe, G. Proust, E.K. Cerreta, A. Misra, Quantitative analysis of deformation twinning in zirconium, Int. J. Plast. 25 (2009) 454–472.
[16] I.J. Beyerlein, C.N. Tomé, A probabilistic twin nucleation model for HCP polycrystalline metals, Proc. R. Soc. A Math. Phys. Eng. Sci. 466 (2010) 2517–2544, http://dx.doi.org/10.1098/rspa.2009.0661. URL, http://rspa.royalsocietypublishing.org/cgi/doi/10.1098/rspa.2009.0661.
[17] S.R. Agnew, C.N. Tomé, D.W. Brown, T.M. Holden, S.C. Vogel, Study of slip mechanisms in a magnesium alloy by neutron diffraction and modeling, Scr. Mater. 48 (2003) 1003–1008.
[18] D.W. Brown, S.R. Agnew, M.A.M. Bourke, T.M. Holden, S.C. Vogel, C.N. Tomé, Internal strain and texture evolution during deformation twinning in magnesium, Mater. Sci. Eng. A 399 (2005) 1–12.
[19] S.R. Agnew, D.W. Brown, C.N. Tomé, Validating a polycrystal model for the elastoplastic response of magnesium alloy AZ31 using in situ neutron diffraction, Acta Mater. 54 (2006) 4841–4852.
[20] B. Clausen, C.N. Tomé, D.W. Brown, S.R. Agnew, Reorientation and stress relaxation due to twinning: Modeling and experimental characterization for Mg, Acta Mater. 56 (2008) 2456–2468.
[21] C. Aydiner, J.V. Bernier, B. Clausen, U. Lienert, C.N. Tomé, D.W. Brown, Evolution of stress in individual grains and twins in a magnesium alloy aggregate, Phys. Rev. B 80 (2009) 024113.
[22] D. Bhattacharyya, E.K. Cerreta, R.J. McCabe, M. Niewczas, G.T. Gray III, A. Misra, C.N. Tomé, Origin of dislocations within tensile and compressive twins in pure textured Zr, Acta Mater. 57 (2009) 305–315.
[23] I.J. Beyerlein, L. Capolungo, P.E. Marshall, R.J. McCabe, C.N. Tomé, Statistical analyses of deformation twinning in magnesium, Philos. Mag. 90 (2010) 2161–2190.
[24] H. El Kadiri, A.L. Oppedal, D.J. Millard XXXVIII, Twin formation, in cadmium, Lond. Edinb. Dublin Philos. Mag. J. Sci. 43 (Series 7) (1952) 422–440.
[26] B.A. Bilby, A.G. Crocker, The Theory of the Crystallography of Deformation Twinning, Proc. R. Soc. Lond. Ser. A Math. Phys. Eng. Sci. 288 (1965) 240–255, http://dx.doi.org/10.1098/rspa.1965.0216. URL, http://rspa.royalsocietypublishing.org/cgi/doi/10.1098/rspa.1965.0216.
[27] S.G. Song, G.T. Gray III, Structural interpretation of the nucleation and growth of deformation twins in Zr and Till. Tem study of twin morphology and defect reactions during twinning, Acta Metall. Mater. 43 (1995) 2339–2350.
[28] A. Serra, D.J. Bacon, A new model for {10 1 2} twin growth in hcp metals, Philos. Mag. A 73 (1996) 333–343.
[29] A.A. Salem, S.R. Kalidindi, R.D. Doherty, Strain hardening of titanium: role of deformation twinning, Acta Mater. 51 (2003) 4225–4237.
[30] Y.B. Chun, S.H. Yu, S.L. Semiatin, S.K. Hwang, Effect of deformation twinning on microstructure and texture evolution during cold rolling of CP-titanium, Mater. Sci. Eng. A 398 (2005) 209–219.
[31] N. Bozzolo, L. Chan, A.D. Rollett, Misorientations induced by deformation twinning in titanium, J. Appl. Crystallogr. 43 (2010) 596–602.
[32] D. Lahaie, J.D. Embury, M.M. Chadwick, G.T. Gray III, A note on the deformation of fine grained magnesium alloys, Scripta Metall. Mater. 27 (1992) 139–142.
[33] D.R. Chichili, K.T. Ramesh, K.J. Hemker, The high-strain-rate response of alpha-titanium: experiments, deformation mechanisms and modeling, Acta Mater. 46 (1998) 1025–1043.
[34] M.R. Barnett, Z. Keshavarz, A.G. Beer, X. Ma, Non-Schmid behaviour during secondary twinning in a polycrystalline magnesium alloy, Acta Mater. 56 (2008) 5–15.
[35] L. Capolungo, P.E. Marshall, R.J. McCabe, I.J. Beyerlein, C.N. Tomé, Nucleation and growth of twins in Zr: A statistical study, Acta Mater. 57 (2009) 6047–6056.
[36] D.G.L. Prakash, R. Ding, R.J. Moat, I. Jones, P.J. Withers, J. Quinta da Fonseca, M. Preuss, Deformation twinning in Ti-6Al-4V during low strain rate deformation to moderate strains at room temperature, Mater. Sci. Eng. A 527 (2010) 5734–5744.
[37] M. Preuss, J. Quinta da Fonseca, V. Allen, D.G.L. Prakash, M.R. Daymond, Twinning in structural material with a hexagonal close-packed crystal structure, J. Strain Anal. Eng. Des. 45 (2010) 377–390.
[38] F. Coghe, W. Tirry, L. Rabet, D. Schryvers, P. Van Houtte, Importance of twinning in static and dynamic compression of a Ti6Al4V titanium alloy with an equiaxed microstructure, Mater. Sci. Eng. A 537 (2012) 1–10.
[39] C.N. Tomé, I.J. Beyerlein, J. Wang, R.J. McCabe, A multi-scale statistical study of twinning in magnesium, JOM 63 (2011) 19–23.
[40] P.D. Honniball, M. Preuss, D. Rugg, J. Quinta da Fonseca, Grain breakup during elevated temperature deformation of an HCP metal, Metall. Mater. Trans. A 46 (5) (2015) 2143–2156.
[41] L. Wang, P. Eisenlohr, Y. Yang, T.R. Bieler, M.A. Crimp, Nucleation of paired twins at grain boundaries in titanium, Scr. Mater. 63 (2010a) 827–830.
[42] L. Wang, Y. Yang, P. Eisenlohr, T.R. Bieler, M.A. Crimp, D.E. Mason, Twin Nucleation by Slip Transfer across Grain Boundaries in Commercial Purity Titanium, Metall. Mater. Trans. A 41 (2010b) 421–430.
[43] L. Wang, R.I. Barabash, Y. Yang, T.R. Bieler, M.A. Crimp, P. Eisenlohr, W. Liu, G.E. Ice, Experimental Characterization and Crystal Plasticity Modeling of Heterogeneous Deformation in Polycrystalline α-Ti, Metall. Mater. Trans. A 42 (2011) 626–635.
[44] L. Wang, R.I. Barabash, T.R. Bieler, W. Liu, P. Eisenlohr, Study of $${11\ bar{2} 1}$$ Twinning in α-Ti by EBSD and Laue Microdiffraction, Metall. Mater. Trans. A 44 (2013) 3664–3674.
[45] C.D. Barrett, H. El Kadiri, M.A. Tschopp, Breakdown of the Schmid law in homogeneous and heterogeneous nucleation events of slip and twinning in magnesium, J. Mech. Phys. Solids 60 (2012) 2084–2099.
[46] J. Luster, M.A. Morris, Compatibility of deformation in two-phase Ti-Al alloys: Dependence on microstructure and orientation relationships, Metall. Mater. Trans. A 26 (1995) 1745–1756.
[47] W.A.T. Clark, R.H. Wagoner, Z.Y. Shen, T.C. Lee, I.M. Robertson, H.K. Birnbaum, On the criteria for slip transmission across interfaces in polycrystals, Scripta Metall. Mater. 26 (1992) 203–206.
[48] M.R. Daymond, H.G. Priesmeyer, Elastoplastic deformation of ferritic steel and cementite studied by neutron diffraction and self-consistent modelling, Acta Mater. 50 (2002) 1613–1626.
[49] A.M. Korsunsky, K.E. James, M.R. Daymond, Intergranular stresses in polycrystalline fatigue: Diffraction measurement and self-consistent modelling, Eng. Fract. Mech. 71 (2004) 805–812.
[50] M.R. Daymond, M. Preuss, B. Clausen, Evidence of variation in slip mode in a polycrystalline nickel-base superalloy with change in temperature from

neutron diffraction strain measurements, Acta Mater. 55 (2007) 3089–3102.
[51] F. Xu, R.A. Holt, M.R. Daymond, R.B. Rogge, E.C. Oliver, Development of internal strains in textured Zircaloy-2 during uni-axial deformation, Mater. Sci. Eng. A 488 (2008) 172–185.
[52] S. Cai, M.R. Daymond, R.A. Holt, M.A. Gharghouri, E.C. Oliver, Evolution of interphase and intergranular stresses in Zr2.5Nb during room temperature deformation, Mater. Sci. Eng. A 501 (2009) 166–181.
[53] M. Kerr, M.R. Daymond, R.A. Holt, J.D. Almer, Mapping of crack tip strains and twinned zone in a hexagonal close packed zirconium alloy, Acta Mater. 58 (2010) 1578–1588.
[54] B.C. Larson, W. Yang, G.E. Ice, J.D. Budai, J.Z. Tischler, Three-dimensional X-ray structural microscopy with submicrometre resolution, Nature 415 (2002) 887–890.
[55] W. Liu, J.N. DuPont, Fabrication of carbide-particle-reinforced titanium aluminide-matrix composites by laser-engineered net shaping, Metall. Mater. Trans. A 35 (2004) 1133–1140.
[56] W. Liu, G.E. Ice, B.C. Larson, W. Yang, J.Z. Tischler, Nondestructive three-dimensional characterization of grain boundaries by X-ray crystal microscopy, Ultramicroscopy 103 (2005) 199–204.
[57] G.E. Ice, R.I. Barabash, White Beam Microdiffraction and Dislocations Gradients, in: F.R.N. Nabarro, J.P. Hirth (Eds.), Dislocations in Solids, volume 13, Elsevier B.V., 2007, pp. 499–601, http://dx.doi.org/10.1016/S1572-4859(07)80011-8. URL, http://www.sciencedirect.com/science/article/pii/S1572485907800118.
[58] H.F. Poulsen, S. Garbe, T. Lorentzen, D. Juul Jensen, F.W. Poulsen, N.H. Andersen, T. Frello, R. Feidenhans'l, H. Graafsma, Applications of high-energy synchrotron radiation for structural studies of polycrystalline materials, J. synchrotron Radiat. 4 (1997) 147–154.
[59] H.F. Poulsen, S.F. Nielsen, E.M. Lauridsen, S. Schmidt, R.M. Suter, U. Lienert, L. Margulies, T. Lorentzen, D. Juul Jensen, Three-dimensional maps of grain boundaries and the stress state of individual grains in polycrystals and powders, J. Appl. Crystallogr. 34 (2001) 751–756.
[60] E.M. Lauridsen, S. Schmidt, R.M. Suter, H.F. Poulsen, Tracking: a method for structural characterization of grains in powders or polycrystals, J. Appl. Crystallogr. 34 (2001) 744–750.
[61] H.F. Poulsen, Three-dimensional X-Ray Diffraction Microscopy: Mapping Polycrystals and Their Dynamics, Springer, 2004. URL, http://books.google.fr/books?id=_jzrH20Qu6cC.
[62] H.F. Poulsen, An introduction to three-dimensional X-ray diffraction microscopy, J. Appl. Crystallogr. 45 (2012) 1084–1097.
[63] W. Ludwig, P. Reischig, A. King, M. Herbig, E.M. Lauridsen, G. Johnson, J. Marrow, J.-Y. Buffière, Three-dimensional grain mapping by x-ray diffraction contrast tomography and the use of Friedel pairs in diffraction data analysis, Rev. Sci. Instrum. 80 (2009) 033905.
[64] P. Reischig, A. King, L. Nervo, N. Viganò, Y. Guilhem, W.J. Palenstijn, K.J. Batenburg, M. Preuss, W. Ludwig, Advances in X-ray diffraction contrast tomography: flexibility in the setup geometry and application to multiphase materials, J. Appl. Crystallogr. 46 (2013) 297–311.
[65] C. Guo, R. Xin, C. Ding, B. Song, Q. Liu, Understanding of variant selection and twin patterns in compressed Mg alloy sheets via combined analysis of Schmid factor and strain compatibility factor, Mater. Sci. Eng. A 609 (2014) 92–101.
[66] T.R. Bieler, L. Wang, A.J. Beaudoin, P. Kenesei, U. Lienert, In Situ Characterization of Twin Nucleation in Pure Ti Using 3D-XRD, Metall. Mater. Trans. A 45 (2014a) 109–122.
[67] T.R. Bieler, P. Eisenlohr, C. Zhang, H.J. Phukan, M.A. Crimp, Grain boundaries and interfaces in slip transfer, Curr. Opin. Solid State Mater. Sci. 18 (2014b) 212–226.
[68] Y. Guo, T.B. Britton, A.J. Wilkinson, Slip bandgrain boundary interactions in commercial-purity titanium, Acta Mater. 76 (2014) 1–12.
[69] A. Fitzner, J. Quinta da Fonseca, J. Kelleher, M. Pascal, D.G.L. Prakash, M. Thomas, S.-Y. Zhang, M. Preuss, The effect of Aluminium on twin activity in binary α-Ti, Acta Mater. 103 (2016) 341–351.
[70] T. Pirling, G. Bruno, P.J. Withers, SALSA-A new instrument for strain imaging in engineering materials and components, Mater. Sci. Eng. A 437 (2006) 139–144.
[71] D.J. Hughes, G. Bruno, T. Pirling, P.J. Withers, Scientific Review: First Impressions of SALSA: The New Engineering Instrument at ILL, Neutron News 17 (2006) 28–32.
[72] J.-C. Labiche, O. Mathon, S. Pascarelli, M.A. Newton, G.G. Ferre, C. Curfs, G.B.M. Vaughan, A. Homs, D.F. Carreiras, The fast readout low noise camera as a versatile x-ray detector for time resolved dispersive extended x-ray absorption fine structure and diffraction studies of dynamic problems in materials science, chemistry, and catalysis, Rev. Sci. Instrum. 78 (2007) 91301.
[73] W.J. Palenstijn, K.J. Batenburg, J. Sijbers, Performance improvements for iterative electron tomography reconstruction using graphics processing units (GPUs), J. Struct. Biol. 176 (2011) 250–253.
[74] W.J. Palenstijn, K.J. Batenburg, J. Sijbers, in: The ASTRA Tomography Toolbox in 13th International Conference on Computational and Mathematical Methods in Science and Engineering, 2013, pp. 1–7. URL, http://www.visielab.ua.ac.be/sites/default/files/cmmse2013.pdf.
[75] U.F. Kocks, C.N. Tomé, H.R. Wenk, Texture and Anisotropy: Preferred Orientations in Polycrystals and Their Effect on Materials Properties, Cambridge University Press, New York, NY, USA, 1998. URL, http://books.google.fr/books?id=vkyU9KZBTioC.
[76] M.R. Barnett, Z. Keshavarz, A.G. Beer, D. Atwell, Influence of grain size on the compressive deformation of wrought Mg-3Al-1Zn, Acta Mater. 52 (2004) 5093–5103.
[77] N. Stanford, U. Carlson, M.R. Barnett, Deformation Twinning and the HallPetch Relation in Commercial Purity Ti, Metall. Mater. Trans. A 39 (2008) 934–944.
[78] W.F. Hosford, The Mechanics of Crystals and Textured Polycrystals, Oxford University Press, New York, NY, USA, 1993.
[79] M.R. Barnett, A rationale for the strong dependence of mechanical twinning on grain size, Scr. Mater. 59 (2008) 696–698.
[80] K. Okazaki, H. Conrad, Effects of interstitial content and grain size on the strength of titanium at low temperatures, Acta Metall. 21 (1973) 1117–1129.
[81] R.W. Armstrong, P.J. Worthington, A Constitutive Relation for Deformation Twinning in Body Centered Cubic Metals, in: R.W. Rohde, B.M. Butcher, J.R. Holland, C.H. Karnes (Eds.), Metallurgical Effects at High Strain Rates, Springer US, Boston, MA, USA, 1973, pp. 401–414, http://dx.doi.org/10.1007/978-1-4615-8696-8. URL, http://www.springerlink.com/index/10.1007/978-1-4615-8696-8.
[82] S.G. Song, G.T. Gray III, Structural interpretation of the nucleation and growth of deformation twins in Zr and Til. Application of the coincidence site lattice (CSL) theory to twinning problems in h.c.p. structures, Acta Metall. Mater. 43 (1995) 2325–2337.
[83] M.R. Barnett, M.D. Nave, A. Ghaderi, Yield point elongation due to twinning in a magnesium alloy, Acta Mater. 60 (2012) 1433–1443.
[84] A. Fernández, A. Jérusalem, I. Gutiérrez-Urrutia, M.T. Pérez-Prado, Three-dimensional investigation of grain s interactions in a Mg AZ31 alloy by electron backscatter diffraction and continuum modeling, Acta Mater. 61 (2013) 7679–7692.
[85] R. Xin, C. Guo, Z. Xu, G. Liu, X. Huang, Q. Liu, Characteristics of long {10-12} twin bands in sheet rolling of a magnesium alloy, Scr. Mater. 74 (2014) 96–99.
[86] G. Timár, J. Quinta da Fonseca, Modeling Twin Clustering and Strain Localization in Hexagonal Close-Packed Metals, Metall. Mater. Trans. A 45 (2014) 5883–5890.